

Role of ZnO Electron-Selective Layers in Regular and Inverted Bulk Heterojunction Solar Cells

Pablo P. Boix,[†] Jon Ajuria,[‡] Ikerne Etxebarria,[‡] Roberto Pacios,[‡] Germà Garcia-Belmonte,^{*,†} and Juan Bisquert[†]

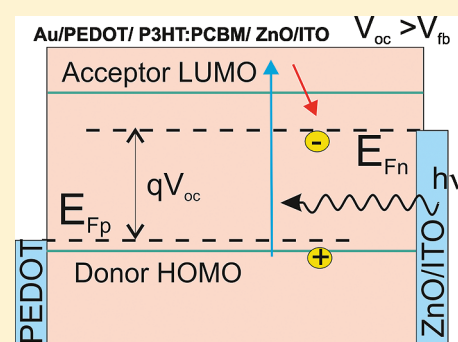
[†]Photovoltaic and Optoelectronic Devices Group, Departament de Física, Universitat Jaume I, ES-12071 Castelló, Spain

[‡]Department of Microsystems, IKERLAN-IK4, S. Coop. Goiru Kalea 9, Polo Innovación Garaia, ES-20500 Arrasate-Mondragón, Gipuzkoa, Spain

S Supporting Information

ABSTRACT: Here the role of metal oxide (ZnO) electron-selective layers in the operating mechanisms of bulk-heterojunction polymer–fullerene solar cells is addressed. Inverted as well as regular structures containing ZnO layers at the cathode contact have been analyzed using capacitance methods in the dark and impedance spectroscopy under illumination. We systematically observed that the open-circuit voltage V_{oc} at 1 sun illumination results higher for inverted cells than that achieved by regular structures in $\Delta V_{oc} \approx 30\text{--}50\text{ mV}$. This shift correlates with the displacement of the flat-band potential V_{fb} extracted from Mott–Schottky capacitance analysis. A coherent picture is provided that states the hole Fermi level of the polymer highest occupied molecular orbital as an energy reference for both V_{oc} and V_{fb} . The study connects the position of the hole Fermi level to the *p*-doping character of the active layer that is influenced by the film morphology through vertical phase segregation.

SECTION: Energy Conversion and Storage



Organic bulk-heterojunction solar cells comprising a low work function cathode metal degrade rapidly without proper encapsulation because of oxidation of the highly reactive electrode. One approach to overcome this problem has been the deposition of metal oxide buffer layers (ZnO, TiO₂) onto indium tin oxide (ITO) substrate as an electron collecting contact.^{1,2} This approach requires an inversion in the ordering of layer deposition allowing for more stable metals such as Ag or Au to be used as back hole collecting electrodes. Metal oxide layers have the additional effect of acting as a hole blocking contact, along with enhancing electron extraction. Although the air-stability of inverted, non-encapsulated structures has been largely demonstrated,³ it is still unclear whether a ZnO layer modifies the inner operating mechanisms of the solar devices.

With the aim of discerning the effect of ZnO electron-selective layers on the overall performance of organic bulk-heterojunction solar cells, we prepared a series of devices with inverted structure (ITO/ZnO/P3HT:PCBM/PEDOT:PSS/Au) (where P3HT = poly-3(hexylthiophene), PCBM = [6,6]-phenyl-C₆₁-butyric acid methyl ester, PEDOT = poly(3,4-ethylenedioxythiophene), and PSS = poly(styrene sulfonate)), in which the polymer/fullerene blend was deposited on top of the cathode; and another series of devices with regular structure (ITO/PEDOT:PSS/P3HT:PCBM/ZnO/Ag) with the blend deposited on top of the anode, and a ZnO-covered cathode. Both kinds of devices comprise a similar cathode structure formed by ZnO layers, with the main

difference being the deposition order: whereas for inverted structures the cathode is deposited first, regular structure deposition starts by spin-coating the hole-transporting PEDOT layer making up the device anode. Details on the solar cells construction were published elsewhere.⁴ An example of the usually obtained *J*–*V* characteristics is plotted in Figure 1, along with basic energy diagrams of both devices. We systematically observed that the open-circuit voltage V_{oc} at 1 sun illumination results higher for inverted cells than that achieved by regular structures (see Table 1). Such a difference attains values within the range of $\Delta V_{oc} \approx 30\text{--}50\text{ mV}$. The resulting power conversion efficiency was observed to lie within the range of $\eta = 2.5\text{--}3.0\%$, always larger in the case of inverted solar cells. The short-circuit current J_{sc} did not exhibit any systematic variation. Since the same P3HT:PCBM active layer is used in both devices, and similar ZnO buffer layers modify the cathode structure, the systematic shift in V_{oc} is in principle not expected and should somehow be related to the change in layer deposition order.

To gain some insight into such a difference in open-circuit voltage ΔV_{oc} between regular and inverted structures, we measure capacitance–voltage characteristics *C*–*V* (Figure 2a), which has been related to the formation of a depletion zone in the

Received: January 11, 2011

Accepted: January 28, 2011

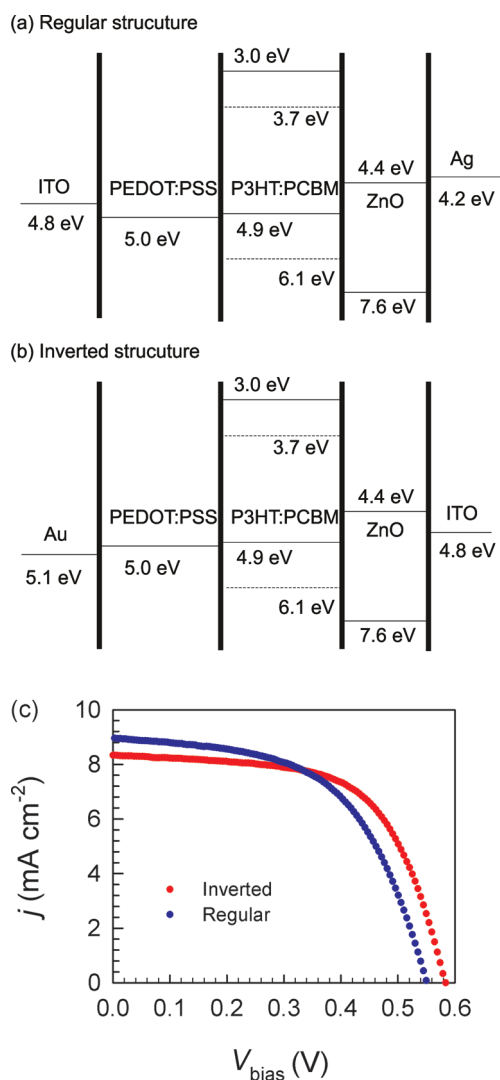


Figure 1. Approximated energy level diagram for the regular (a) and inverted (b) structures studied. (c) Current density–voltage characteristics of typical devices under standard AM1.5G illumination conditions (1000 W m^{-2} of integrated power density).

Table 1. Photovoltaic and Operating Parameters of Regular (ITO/PEDOT/P3HT:PCBM/ZnO/Ag) and Inverted (ITO/ZnO/P3HT:PCBM/PEDOT/Au) Structures^a

	J_{sc} (mA cm ⁻²)	V_{oc} (mV)	η (%)	FF	V_{fb} (mV)	N (10^{16} cm^{-3})	w (nm)
regular	8.96	550	2.73	0.554	315	1.6	81
inverted	8.33	584	2.99	0.616	356	6.1	44

^a Depletion-zone width w corresponds to zero bias.

vicinity of the cathode contact.⁵ The capacitance in reverse and low-forward bias relates to the width of the depletion zone, which is modulated by changing the applied voltage. As a consequence, the electrical field is confined near the cathode, and band bending appears with a corresponding majority-carrier depletion,^{5,6} due to the presence of acceptor defects (see Figure 3c,d). Inherent energetic disorder of organic semiconductors resulting from structural inhomogeneities or chemical impurities enhances charge localization and gives rise to carrier trapping. Negatively charged defects (acceptor states) donate a hole to the transport-related

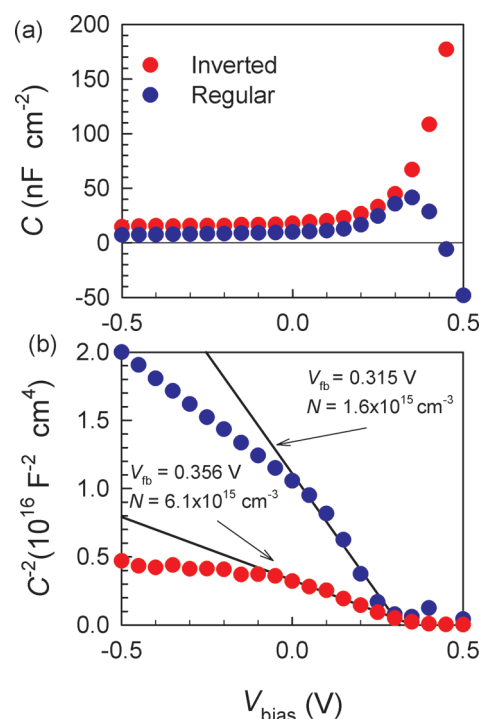


Figure 2. (a) Comparison of capacitance–voltage response of regular and inverted devices. Capacitance measured in the dark and at room temperature at 100 Hz. (b) Mott–Schottky characteristics of the solar cells exhibiting a linear relationship (straight lines) at low forward bias (0–0.4 V). Flat-band potential V_{fb} and doping level N are indicated for each curve.

highest occupied molecular orbital (HOMO) levels and are then responsible for the p -doping of the polymer. In addition, it is known that P3HT is a conjugated polymer that, upon exposure to oxygen⁷ or moisture,⁸ becomes p -doped, exhibiting relatively high levels of free carriers (10^{15} – 10^{17} cm^{-3}).⁹ Capacitance measurements have been used to evidence such band bending^{10–12} usually exhibiting Mott–Schottky characteristics as shown in Figure 2b, $C^{-2} = (2/q\varepsilon N)(V_{\text{fb}} - V)$, where $\varepsilon \approx 3\varepsilon_0$ is the permittivity of the blend, N is the doping level, and q is the elementary charge. A similar C – V relationship has been recently shown in analyzing bulk heterojunction/electrolyte interfaces.¹³

A diagram of the contact energetics is depicted in Figure 3: before contact there exists an energy level offset between the doped polymer ϕ_s and the contact ϕ_c . Here $\phi_s = E_{\text{F0}}$ stands for the polymer/fullerene work function (Fermi level), which is located near the polymer HOMO level because of the p -doping, and ϕ_c corresponds to the contact work function as in Figure 3a, b. It is assumed that the cathode work function is determined by the inclusion of the ZnO layer in both cases. After contact, the band bending compensates the work function mismatch, and such a difference relates to the flat-band potential as $qV_{\text{fb}} = \phi_c - \phi_s$, as shown in the equilibrium conditions of Figure 3c,d. It is assumed that the anodes always form ohmic contacts by aligning E_{F0} to the HOMO of the hole-transporting, conductive PEDOT layer. Mott–Schottky analysis in Figure 2b allows determining both the flat-band potential from the intercept of the linear relation with the voltage axis, and simultaneously the doping level from the $C^{-2} \propto V$ slope. Explanations on the Mott–Schottky analysis can be found in previous papers.⁵ We observe that inverted cells exhibit higher V_{fb} than that found for regular cells,

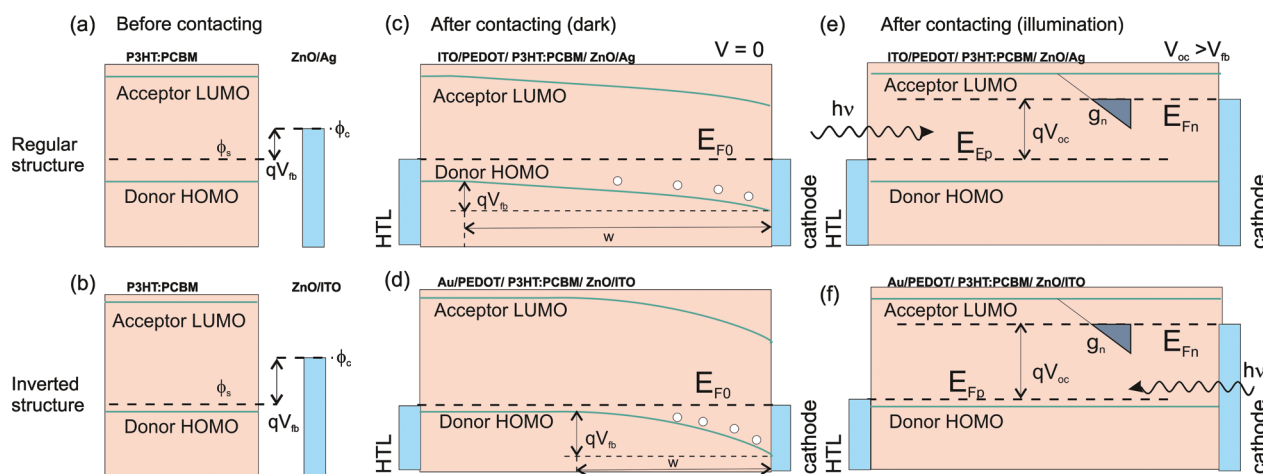


Figure 3. Energy diagram representing donor HOMO and acceptor lowest unoccupied molecular orbitals (LUMO) levels, the active layer work function ϕ_s , and the ZnO-cathode work function ϕ_c for regular (a) and inverted (b) structures before contacting. For inverted devices, ϕ_s is positioned closer to the donor HOMO because of higher doping. (c,d) Band diagram of a *p*-doped donor polymer–acceptor fullerene blend at zero bias voltage (in the dark). A depletion zone of width w is formed at the cathode, and an ohmic contact at the hole transporting layer (HTL) interface. Work function offset (V_{fb}) produces a band-bending by Fermi level alignment E_{F0} . (e,f) Band diagram under illumination, and open-circuit conditions producing $V_{oc} > V_{fb}$. The Fermi level splitting accounts for V_{oc} . The same electron occupation (filled area of g_n) occurs, being the only change in the shift of the hole Fermi level E_{Fp} between regular and inverted structures. In all the diagrams the same energy scale is adopted.

in such a way that $\Delta V_{fb} \approx 30\text{--}40$ mV (see Table 1). This flat-band shift is found to correlate with the open-circuit voltage difference mentioned previously. The density of dopants turns out to be larger for inverted cells, $N_i = 6.1 \times 10^{16} \text{ cm}^{-3}$, in comparison with regular cells, $N_r = 1.6 \times 10^{16} \text{ cm}^{-3}$, by a factor 6, which establishes the dark hole density p_0 . Because the $C^{-2} \propto V$ relation is obeyed at voltages approaching V_{fb} , the doping level extracted corresponds to the charge density in the vicinity of the cathode contact. Such a difference in doping density implies a shift of the Fermi level E_{F0} (polymer work function) for the inverted cells approaching the polymer HOMO level, which can be approximated by an amount equal to $k_B T \ln(N_i/N_r)$. Here $k_B T$ stands for the thermal energy. Again a shift of about 30–40 mV is obtained, which is fully consistent with the displacement of the flat-band potential. In Figure 3 both situations are compared: increase in doping moves the Fermi level down (approaching the polymer HOMO) in the case of inverted cells. We derive thereby that the shift in flat-band potential $q\Delta V_{fb} \approx \Delta E_{F0} = k_B T \ln(N_i/N_r)$ appears as a consequence of the polymer Fermi level displacement.

Another important point resulting from the Mott–Schottky analysis is that the depletion zone width at zero bias $w = (2\epsilon V_{fb}/qN)^{1/2}$ practically reaches the anode ($w = 81$ nm) for the regular structure, whereas it is limited to half the active layer thickness ($w = 44$ nm) in the case of an inverted cell (Figure 3c,d). This is mainly because of the difference in doping between both kinds of structures: more doped layers confine the electrical field in the vicinity of the cathode. We observe then that the change in deposition order of the active layer is responsible for the displacement of the equilibrium Fermi level by modification of *p*-doping. We later discuss the origin for such a variation in polymer doping.

In order to further understand the reasons behind the reported observation $\Delta V_{fb} \approx \Delta V_{oc}$ we next need to introduce the relation between the output open-circuit voltage and the charge carrier Fermi levels under illumination. In every solar cell, the open-circuit photovoltage that can be achieved by a given material or blend is equal to the difference between the electron and hole

chemical potentials (quasi-Fermi levels) in the absorbing layer under steady-state illumination.^{14,15}

$$qV_{oc} = E_{Fn} - E_{Fp} \quad (1)$$

Hence the output voltage measured in open-circuit conditions monitors the splitting of the Fermi levels, which in turn are stated by the charge-carrier concentrations after thermalization into lower lying states. This idea is drawn in Figure 3e,f, where qV_{oc} is the free energy distance between carrier (electron and hole) Fermi levels. Since the polymer is *p*-doped to some extent, the downward shift of E_{Fp} by effect of illumination should be restricted within $k_B T$. This is because the amount of excess, photo-generated holes for usual illumination intensities near 1 sun lies within the order of magnitude of the density of dopants $p_0 \approx \Delta p = 10^{16}\text{--}10^{17} \text{ cm}^{-3}$.¹⁶ Photogeneration then moves the electron Fermi level E_{Fn} upward, while slightly displacing the hole Fermi level downward. As a consequence, E_{Fp} acts as an energy reference for V_{oc} . This last statement implies that ΔV_{oc} is expected to follow $\Delta E_{Fp}/q \approx \Delta V_{fb}$, in good accordance with our reported observation.

A useful manner to corroborate the proposed explanation for the origin of the V_{oc} shift consists in measuring impedance spectroscopy at different illumination intensities in open-circuit conditions, as reported recently.¹⁷ The applied bias voltage compensates for the effect of the photovoltage so that the cell is effectively measured at open-circuit, i.e., photocurrent is canceled by the recombination flow and $j_{dc} = 0$. Such measuring conditions allow focusing on nongeminate recombination mechanisms, which have been identified as the dominant loss effect near V_{oc} .^{16–18} The impedance spectra are characterized by a major, low-frequency RC arc plus additional minor features at high frequency (see Supporting Information).^{17,19} This low frequency arc is attributed to the processes of photogenerated carrier recombination (resistance R_{rec}) and storage (chemical capacitance C_μ) in the photoactive blend.²⁰ The chemical capacitance parameter extracted from impedance is shown in Figure 4a. From the capacitance dependence on V_{oc} , it is feasible to estimate the charge carrier density by integration of the

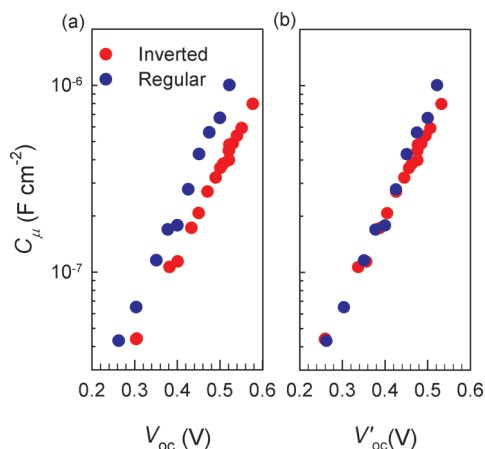


Figure 4. (a) Chemical capacitance extracted from impedance spectroscopy analysis. An exponential dependence on V_{oc} as $C_\mu \propto \exp(\alpha V_{oc}/k_B T)$, with $\alpha = 0.26$, is obtained. (b) Same data after correcting the voltage axis $V'_{oc} = V_{oc} - \Delta V_{oc}$, only in the case of inverted structure.

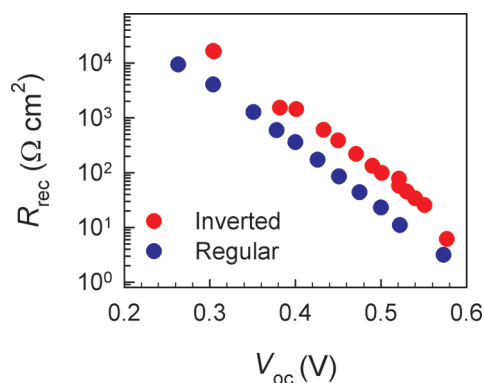


Figure 5. Recombination resistance extracted from impedance spectroscopy analysis. An exponential dependence on V_{oc} as $R_{rec} \propto \exp(-\beta V_{oc}/k_B T)$, with $\beta = 0.65$, is observed.

$C_\mu(V_{oc})$ curve, which is in fact a representation of the electron density-of-states (DOS) as $C_\mu = q^2 g_n(V_{oc})$.^{17,21} Gaussian¹⁷ as well as exponential²² DOS have been proposed, accounting for the electron state distribution, although it is hard to distinguish between them in practical experiments because illumination intensities are only able to reach low-occupancy conditions (10^{14} – 10^{17} cm^{-3}). Dependences of capacitance on V_{oc} in Figure 4 exhibit exponential laws as $C_\mu \propto \exp(\alpha V_{oc}/k_B T)$, with $\alpha \approx 0.26$ in both cases. In Figure 4b, we represent the same data using a corrected voltage axis as $V'_{oc} = V_{oc} - \Delta V_{oc}$, only in the case of the inverted structure. By examining Figure 4b, one can realize that both capacitances coincide, thus indicating that the voltage shift is only produced by a shift in energy reference E_{FP} . The fact that the capacitance–voltage characteristics in Figure 4 collapse into a unique curve after correction of the energy shift implies that the same electron DOS occupation occurs by effect of the light (see Figure 3e,f). As a consequence, we conclude that the inner operation mechanisms of the solar cell bulk are not altered by inversion of the deposition order. The same kind of argument can be employed to account for the displacement in recombination resistance of Figure 5. As expected, recombination

resistance also follows an exponential dependence on photo-voltage as $R_{rec} \propto \exp(-\beta V_{oc}/k_B T)$, with $\beta = 0.65$.

The question about the different doping levels found between inverted and regular structures remains unsolved. It is worth recalling that the main difference during the cell processing is the change of the electrodes: for regular cells, the blend is spin-coated on top of the anode, whereas for inverted cells it is deposited on top of the cathode. Vertical modifications of the blend morphology might be then behind the observed difference in doping level.² It has been reported that polymer and fullerene phases within the blend tend to segregate in the vertical direction after deposition.²³ Fullerene molecules concentrate to some extent at the device bottom to form an acceptor-rich region near the anode in the case of regular cells, or in the vicinity of the cathode for inverted-type structures. We can suggest that, in addition to structural defects acting as acceptor levels, a fullerene-rich zone could be able to capture more electrons in trap states then releasing holes to the polymer HOMO levels, and consequently enhancing doping levels. Since a fullerene-rich zone develops near the cathode of inverted structures, higher doping levels are expected in this case. This would help one understand the relation between active film morphology and electrical parameters.

We have presented a coherent picture describing the operating energetics of organic bulk-heterojunction solar cells. The key point is the observation that the hole Fermi level in dark conditions E_{F0} determines both the flat-band potential, extracted from the usual Mott–Schottky analysis of the reverse and low-forward capacitance, as well as the achievable open-circuit voltage. This is because E_{F0} can be considered as a reference for energies within the device. We have also pointed out that the actual E_{F0} position is linked to the amount of negatively charged defects that donate holes to the polymer HOMO levels, then displace E_{F0} downward and approach the HOMO manifold. This last observation opens the possibility of performing chemically modified defect engineering aiming to control the position of the hole Fermi level, which goes beyond the unintended doped devices on which we have based our study.

EXPERIMENTAL SECTION

Impedance spectroscopy measurements were performed with an Autolab PGSTAT-30 equipped with a frequency analyzer module. AC oscillating amplitude was as low as 20 mV (rms) to maintain the linearity of the response. Measurements were performed always at room temperature either in dark conditions at different bias voltages (Mott–Schottky analysis), or at zero current conditions by applying a bias that equals V_{oc} at varying continuous irradiation intensity (chemical capacitance and recombination resistance). See Supporting Information.

ASSOCIATED CONTENT

S Supporting Information. Figure S1 shows an example of impedance spectroscopy spectra registered in open-circuit conditions at different white light illumination intensities. This material is available free of charge via the Internet <http://pubs.acs.org>.

AUTHOR INFORMATION

Corresponding Author

*E-mail: garciag@fca.uji.es.

ACKNOWLEDGMENT

We acknowledge financial support from Ministerio de Educación y Ciencia under Project HOPE CSD2007-00007 (Consolider-Ingenio 2010), Generalitat Valenciana (Prometeo/2009/058), and Universitat Jaume I (P1.1B2008-32).

REFERENCES

- (1) White, M. S.; Olson, D. C.; Shaheen, S. E.; Kopidakis, N.; Ginley, D. S. Inverted Bulk-Heterojunction Organic Photovoltaic Device Using a Solution-Derived ZnO Underlayer. *Appl. Phys. Lett.* **2006**, *89*, 143517.
- (2) Chen, L.-M.; Hong, Z.; Li, G.; Yang, Y. Recent Progress in Polymer Solar Cells: Manipulation of Polymer:Fullerene Morphology and the Formation of Efficient Inverted Polymer Solar Cells. *Adv. Mater.* **2009**, *21*, 1–16.
- (3) Hau, S. K.; Yip, H.-L.; Baek, N. S.; Zou, J.; O'Malley, K.; Jen, A. K.-Y. Air-Stable Inverted Flexible Polymer Solar Cells Using Zinc Oxide Nanoparticles as an Electron Selective Layer. *Appl. Phys. Lett.* **2008**, *92*, 253301.
- (4) Ajuria, J.; Etxebarria, I.; Cambarau, W.; Muñecas, U.; Tena-Zaera, R.; Jimeno, J. C.; Pacios, R. Inverted ITO-Free Organic Solar Cells Based on p and n Semiconducting Oxides. New Designs for Integration in Tandem Cells, Top or Bottom Detecting Devices, and Photovoltaic Windows. *Energy Environ. Sci.* [Online early access]. DOI: 10.1039/C0EE00318B.
- (5) Garcia-Belmonte, G.; Munar, A.; Barea, E. M.; Bisquert, J.; Ugarte, I.; Pacios, R. Charge Carrier Mobility and Lifetime of Organic Bulk Heterojunctions Analyzed by Impedance Spectroscopy. *Org. Electron.* **2008**, *9*, 847–851.
- (6) Dennler, G.; Lungenschmied, C.; Saricifti, N. S.; Schwödau, R.; Bauer, S.; Reiss, H. Unusual Electromechanical Effects in Organic Semiconductor Schottky Contacts: Between Piezoelectricity and Electrostriction. *Appl. Phys. Lett.* **2005**, *87*, 163501.
- (7) Abdou, M. S. A.; Orfino, F. P.; Son, Y.; Holdcroft, S. Interaction of Oxygen with Conjugated Polymers: Charge Transfer Complex Formation with Poly(3-alkylthiophenes). *J. Am. Chem. Soc.* **1997**, *119*, 4518–4524.
- (8) Hoshino, S.; Yoshida, M.; Uemura, S.; Kodzasa, T.; Takada, N.; Kamata, T.; Yase, K. Influence of Moisture on Device Characteristics of Polythiophene-Based Field-Effect Transistors. *J. Appl. Phys.* **2004**, *95*, 5088–5093.
- (9) Liang, Z.; Nardes, A.; Wang, D.; Berry, J. J.; Gregg, B. A. Defect Engineering in π -Conjugated Polymers. *Chem. Mater.* **2009**, *21*, 4914–4919.
- (10) Boix, P. P.; Garcia-Belmonte, G.; Muñecas, U.; Neophytou, M.; Waldauf, C.; Pacios, R. Determination of Gap Defect States in Organic Bulk Heterojunction Solar Cells from Capacitance Measurements. *Appl. Phys. Lett.* **2009**, *95*, 233302.
- (11) Bisquert, J.; Garcia-Belmonte, G.; Munar, A.; Sessolo, M.; Soriano, A.; Bolink, H. J. Band Unpinning and Photovoltaic Model for P3HT-PCBM Organic Bulk Heterojunctions under Illumination. *Chem. Phys. Lett.* **2008**, *465*, 57–62.
- (12) Limpinsel, M.; Wagenpfahl, A.; Mingeback, M.; Deibel, C.; Dyakonov, V. Photocurrent in Bulk Heterojunction Solar Cells. *Phys. Rev. B* **2010**, *81*, 085203.
- (13) Gautam, V.; Bag, M.; Narayan, K. S. Dynamics of Bulk Polymer Heterostructure/Electrolyte Devices. *J. Phys. Chem. Lett.* **2010**, *1*, 3277–3282.
- (14) Bisquert, J.; Cahen, D.; Hodes, G.; Rühle, S.; Zaban, A. Physical Chemical Principles of Photovoltaic Conversion with Nanoparticulate, Mesoporous Dye-Sensitized Solar Cells. *J. Phys. Chem. B* **2004**, *108*, 8106–8118.
- (15) Garcia-Belmonte, G.; Bisquert, J. Open-Circuit Voltage Limit Caused by Recombination through Tail States in Bulk Heterojunction Polymer-Fullerene Solar Cells. *Appl. Phys. Lett.* **2010**, *96*, 113301.
- (16) Maurano, A.; Hamilton, R.; Shuttle, C. G.; Ballantyne, A. M.; Nelson, J.; O'Regan, B.; Zhang, W.; McCulloch, I.; Azimi, H.; Morana, M.; et al. Recombination Dynamics as a Key Determinant of Open Circuit Voltage in Organic Bulk Heterojunction Solar Cells: A Comparison of Four Different Donor Polymers. *Adv. Mater.* **2010**, *22*, 4987–4992.
- (17) Garcia-Belmonte, G.; Boix, P. P.; Bisquert, J.; Sessolo, M.; Bolink, H. J. Simultaneous Determination of Carrier Lifetime and Electron Density-of-States in P3HT:PCBM Organic Solar Cells under Illumination by Impedance Spectroscopy. *Sol. Energy Mater. Sol. Cells* **2010**, *94*, 366–375.
- (18) Mauer, R.; Howard, I. A.; Laquai, F. Effect of Nongeminate Recombination on the Fill Factor in Polythiophene/Methanofullerene Organic Solar Cells. *J. Phys. Chem. Lett.* **2010**, *1*, 3500–3505.
- (19) Garcia-Belmonte, G.; Boix, P. P.; Bisquert, J.; Lenes, M.; Bolink, H. J.; La Rosa, A.; Filippone, S.; Martín, N. Influence of the Intermediate Density-of-States Occupancy on Open-Circuit Voltage of Bulk Heterojunction Solar Cells with Different Fullerene Acceptors. *J. Phys. Chem. Lett.* **2010**, *1*, 2566–2571.
- (20) Bisquert, J.; Fabregat-Santiago, F.; Mora-Seró, I.; Garcia-Belmonte, G.; Giménez, S. Electron Lifetime in Dye-Sensitized Solar Cells: Theory and Interpretation of Measurements. *J. Phys. Chem. C* **2009**, *113*, 17278–17290.
- (21) Sánchez-Díaz, A.; Izquierdo, M.; Filippone, S.; Martín, N.; Palomares, E. The Origin of the High Voltage in DPM12/P3HT Organic Solar Cells. *Adv. Funct. Mater.* **2010**, *20*, 2695–2700.
- (22) Shuttle, C. G.; O'Regan, B.; Ballantyne, A. M.; Nelson, J.; Bradley, D. D. C.; de Mello, J.; Durrant, J. R. Experimental Determination of the Rate Law for Charge Carrier Decay in a Polythiophene: Fullerene Solar Cell. *Appl. Phys. Lett.* **2008**, *92*, 093311.
- (23) Campoy-Quiles, M.; Ferenczi, T.; Agostinelli, T.; Etchegoin, P. G.; Kim, Y.; Anthopoulos, T. D.; Stavrinou, P. N.; Bradley, D. D. C.; Nelson, J. Morphology Evolution via Self-Organization and Lateral and Vertical Diffusion in Polymer:Fullerene Solar Cell Blends. *Nat. Mater.* **2008**, *7*, 158–164.